Muon $g-2$ and the B-physics anomalies in RPV supersymmetry and the discovery prospect at LHC and future colliders

Fang Xu

Collaborators: Bhupal Dev, Amarjit Soni
arXiv:2106.15647

Particle Physics on the Plains 2022

Washington University in St. Louis

April 2, 2022

Overview

Motivation

- The recent experimental results of muon $g-2$ (from the Fermilab) and the lepton flavor universality violation in rare B-meson decays (from the LHCb, Belle, BaBar) could be the hints ($> 3\sigma$ anomalies) of new physics beyond the Standard Model.
- RPV3: Assuming the mass of third generation sfermions lighter than the other two generations, RPV3 preserves gauge coupling unification and has the usual attribute of naturally addressing the Higgs radiative stability.
  Altmannshofer, Dev, Soni (PRD 2017).
- Under the minimal RPV supersymmetric framework, muon $g-2$ and the B-physics anomalies could be addressed simultaneously and also could be tested at LHC and beyond.

muon $g-2$ anomaly

- $\Delta a_\mu = a_\mu^{\rm exp} - a_\mu^{\rm SM} = (251 \pm 59) \times 10^{-11}$ has a significance of 4.2σ.
- Could be the signal of new physics beyond the SM where some new couplings to muon could be detectable by LHC or future colliders.

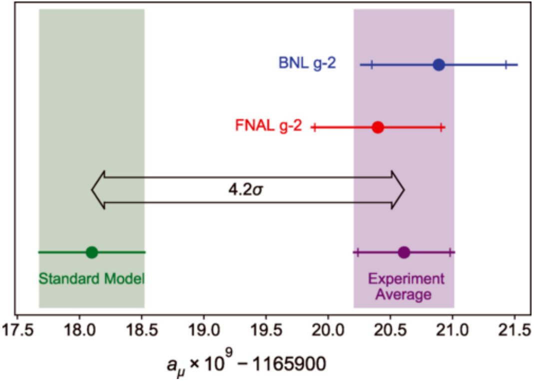

B. Abi et al. (PRL 2021)

B-physics anomalies

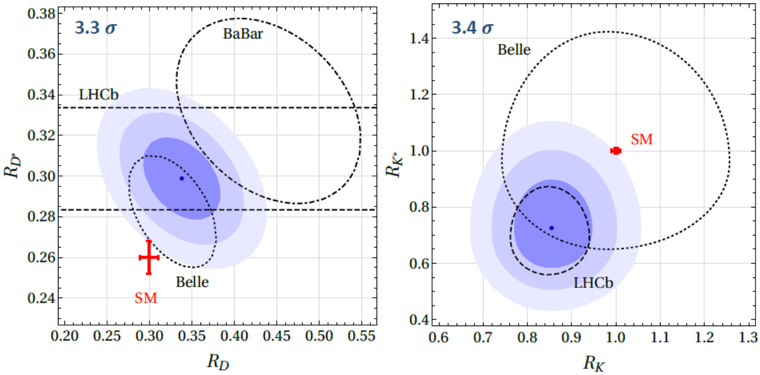

Altmannshofer, Dev, Soni, Sui (PRD 2020)

- $R_{D^{(*)}} = \frac{\text{BR}(B \to D^{(*)}\tau\nu)}{\text{BR}(B \to D^{(*)}\ell\nu)}$ (with $\ell = e, \mu$), $R_{K^{(*)}} = \frac{\text{BR}(B \to K^{(*)}\mu^+\mu^-)}{\text{BR}(B \to K^{(*)}e^+e^-)}$
- Also imply possible new couplings to leptons.

Explanation of anomalies in RPV3 SUSY

- The LQD and LLE part of the RPV SUSY Lagrangian which contains the λ' and λ couplings respectively and are relevant for the $R_{D^{(*)}}$, $R_{K^{(*)}}$ and $(g-2)_\mu$ anomalies.

$$\begin{aligned}\mathcal{L}_{LQD} = \lambda'_{ijk}(&\widetilde{\nu}_{i\mathrm{L}}\overline{d}_{k\mathrm{R}}d_{j\mathrm{L}} + \widetilde{d}_{j\mathrm{L}}\overline{d}_{k\mathrm{R}}\nu_{i\mathrm{L}} + \widetilde{d}^*_{k\mathrm{R}}\overline{\nu}^c_{i\mathrm{L}}d_{j\mathrm{L}} \\ &- \widetilde{e}_{i\mathrm{L}}\overline{d}_{k\mathrm{R}}u_{j\mathrm{L}} - \widetilde{u}_{j\mathrm{L}}\overline{d}_{k\mathrm{R}}e_{i\mathrm{L}} - \widetilde{d}^*_{k\mathrm{R}}\overline{e}^c_{i\mathrm{L}}u_{j\mathrm{L}}) + \mathrm{H.c.}\end{aligned} \tag{1}$$

$$\mathcal{L}_{LLE} = \frac{1}{2}\lambda_{ijk}\left[\widetilde{\nu}_{i\mathrm{L}}\overline{e}_{k\mathrm{R}}e_{j\mathrm{L}} + \widetilde{e}_{j\mathrm{L}}\overline{e}_{k\mathrm{R}}\nu_{i\mathrm{L}} + \widetilde{e}^*_{k\mathrm{R}}\overline{\nu}^c_{i\mathrm{L}}e_{j\mathrm{L}} - (i \leftrightarrow j)\right] + \mathrm{H.c.} \tag{2}$$

- λ couplings are antisymmetric in the first two indices: $\lambda_{ijk} = -\lambda_{jik}$

Explanation of anomalies in RPV3 SUSY

$(g-2)_\mu$ Kim, Kyae, Lee (PLB 2001)

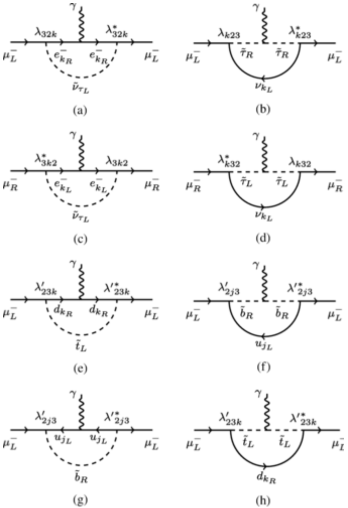

$R_{D^{(*)}}$ Deshpande, He (EPJC 2017); Altmannshofer, Dev, Soni (PRD 2017) etc.

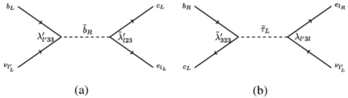

$R_{K^{(*)}}$ Das, Hati, Kumar, Mahajan (PRD 2017); Trifinopoulos (EPJC 2018) etc.

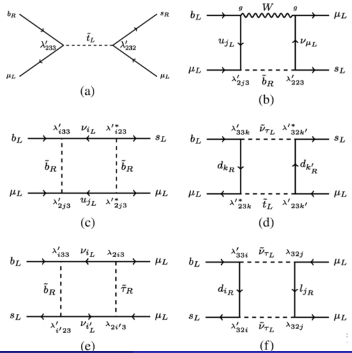

$(g-2)_\mu$

- Following previous discussions (Kim, Kyae, Lee (PLB 2001); Altmannshofer, Dev, Soni, Sui (PRD 2020)), in RPV3 framework, $(g-2)_\mu$ correction can be written as:

$$\Delta a_\mu = \frac{m_\mu^2}{96\pi^2}\sum_{k=1}^{3}\left(\frac{2(|\lambda_{32k}|^2+|\lambda_{3k2}|^2)}{m^2_{\tilde{\nu}_\tau}} - \frac{|\lambda_{3k2}|^2}{m^2_{\tilde{\tau}_{\rm L}}} - \frac{|\lambda_{k23}|^2}{m^2_{\tilde{\tau}_{\rm R}}} + \frac{3|\lambda'_{2k3}|^2}{m^2_{\tilde{b}_{\rm R}}}\right) \quad (3)$$

- $\widetilde{\nu}_\tau$, $\widetilde{\tau}_L$, $\widetilde{\tau}_R$ or $\widetilde{b}_R$ in the loop
- $\widetilde{\tau}_L$, $\widetilde{\tau}_R$: negative contribution. Make $m_{\widetilde{\tau}_{L,R}}$ large
- $\widetilde{\nu}_\tau$, $\widetilde{b}_R$: positive contribution
- $\widetilde{\nu}_\tau$ gives the main contribution in our scenarios

$R_{D^{(*)}}$

- BSM contribution at tree level from the $\widetilde{b}_R$ exchange (contribution from $\widetilde{\tau}_L$ exchange is zero in our scenarios) gives rise to a SM-like effective Hamiltonian:

$$\mathcal{H}_{\text{eff}}^{b\to c\ell\nu} = \frac{4G_F}{\sqrt{2}} V_{cb}\,(1 + C_{V_L})\,\mathcal{O}_{V_L} + \text{H.c.} \tag{4}$$

with the operator $\mathcal{O}_{V_L} = (\bar{c}_L\gamma^\mu b_L)(\bar{\ell}_L\gamma_\mu\nu_{\ell L})$ with a corresponding coefficient $C_{V_L} \simeq 0.09$

- Then we have

$$\frac{R_D}{R_D^{\text{SM}}} = \frac{R_{D^*}}{R_{D^*}^{\text{SM}}} = \frac{|\Delta_{31}^c|^2 + |\Delta_{32}^c|^2 + |1 + \Delta_{33}^c|^2}{|\Delta_{21}^c|^2 + |1 + \Delta_{22}^c|^2 + |\Delta_{23}^c|^2} \tag{5}$$

with $\Delta_{ll'}^c = \frac{v^2}{4m_{\tilde{b}_R}^2}\lambda'_{l'33}\left(\lambda'_{l33} + \lambda'_{l23}\frac{V_{cs}}{V_{cb}} + \lambda'_{l13}\frac{V_{cd}}{V_{cb}}\right)$

$R_{K^{(*)}}$

- The relevant effective Hamiltonian

$$\mathcal{H}_{\text{eff}}^{b\to s\ell\ell} = -\frac{4G_F}{\sqrt{2}} V_{ts}^* V_{tb} \frac{e^2}{16\pi^2} \sum_{i=9,10} \left[C_i^\ell Q_i^\ell + C_i'^\ell Q_i'^\ell \right] \tag{6}$$

with the operators $Q_9^\ell = (\bar{s}\gamma_\alpha P_L b)(\bar{\ell}\gamma^\alpha \ell)$, $Q_{10}^\ell = (\bar{s}\gamma_\alpha P_L b)(\bar{\ell}\gamma^\alpha\gamma_5 \ell)$ and $Q_{9,10} \xrightarrow{P_L \to P_R} Q'_{9,10}$

- The resulting Wilson coefficients (1 loop contribution)

$$C_9^\mu = -C_{10}^\mu = \frac{m_t^2}{m_{\tilde{b}_R}^2} \frac{|\lambda'_{233}|^2}{16\pi\alpha_{\text{em}}} - \frac{v^2}{m_{\tilde{b}_R}^2} \frac{X_{bs} X_{\mu\mu}}{64\pi\alpha_{\text{em}} V_{tb} V_{ts}^*} \tag{7}$$

where $X_{bs} = \sum_{i=1}^3 \lambda'_{i33}\lambda'_{i23}$ and $X_{\mu\mu} = \sum_{j=1}^3 |\lambda'_{2j3}|^2$

- Tree level $\widetilde{t}_L$ exchange $\to$ wrong chirality. Make $m_{\widetilde{t}_L}$ large

Parameter space

- Parameters $(\lambda_{232}, \lambda'_{233}, \lambda'_{223}, \lambda'_{232}, m_{\tilde{b}_{\mathrm{R}}}, m_{\tilde{b}_{\mathrm{L}}}, m_{\tilde{\nu}_\tau}, m_{\tilde{\tau}_{\mathrm{L}}})$
  - $\lambda_{232} = -\lambda_{322} \neq 0 \Leftarrow$ contribute to muon $g-2$, other λ_{3ij} couplings cannot be large at the same time due to the constraints of $\tau \to \mu\mu\mu$, $\mu \to e\gamma$ etc.
  - $\lambda'_{2ij} \neq 0 \Leftarrow$ include μ and free of $m_{\tilde{\nu}_\tau}$.
  - $\lambda'_{3ij} = 0$, otherwise combined with λ_{32k} or λ_{3k2}, well measured meson decays $(\bar{d}_i d_j) \to \mu\ell_k$ or $\tau \to \mu K$ and $\tau \to \mu\eta$ decays will prevent λ'_{3ij} to be large.
  - $m_{\tilde{\tau}_{\mathrm{R}}}$ not involved with this choice of couplings.
  - $m_{\tilde{t}_{\mathrm{L}}}$ can only influence $\mathrm{BR}(B_s \to \mu^+\mu^-)$ and the Wilson coefficients $(C'_9)^\mu$ and $(C'_{10})^\mu$ that describe the $R_{K^{(*)}}$ anomaly. But we can assume a relatively larger value to make the influence small.

Parameter space

- 8-D parameter space $(\lambda_{232}, \lambda'_{233}, \lambda'_{223}, \lambda'_{232}, m_{\tilde{b}_R}, m_{\tilde{b}_L}, m_{\tilde{\nu}_\tau}, m_{\tilde{\tau}_L})$
  - $m_{\tilde{b}_R} = m_{\tilde{b}_L}$ for simplicity.
  - $m_{\tilde{\tau}_L}$ has opposite contribution for $(g-2)_\mu$. The influence is not important as long as $m_{\tilde{\tau}_L} \gtrsim O(2\ \mathrm{TeV})$. Here we choose 4 TeV.
- $\Rightarrow$ 6-D parameter space $(\lambda_{232}, \lambda'_{233}, \lambda'_{223}, \lambda'_{232}, m_{\tilde{b}}, m_{\tilde{\nu}_\tau})$
- In a sense, $(\lambda', m_{\tilde{b}})$ and $(\lambda, m_{\tilde{\nu}_\tau})$ are orthogonal in our scenario since $(\lambda, m_{\tilde{\nu}_\tau})$ can only influence $(g-2)_\mu$ anomaly and 4-lepton constraint while on the other hand, $(\lambda', m_{\tilde{b}})$ can only influence $R_{D^{(*)}}$ and $R_{K^{(*)}}$ anomalies and other constraints (The influence to $(g-2)_\mu$ is very small because $m^2_{\tilde{b}} \gg m^2_{\tilde{\nu}_\tau}$ as we will see from Fig(d)(e)(g)).
- So, we can plot the constraints and anomalies in two 2-D spaces: $(\lambda', m_{\tilde{b}})$ and $(\lambda, m_{\tilde{\nu}_\tau})$

Numerical scan

- We scan the 6-D parameter space $(\lambda_{232}, \lambda'_{233}, \lambda'_{223}, \lambda'_{232}, m_{\tilde{b}_{\rm R}} = m_{\tilde{b}_{\rm L}}, m_{\tilde{\nu}_\tau}, m_{\tilde{\tau}_{\rm L}} = 4\ \text{TeV})$
- $m_{\tilde{\nu}_\tau} \in [0.7, 1.2]$ TeV (also tried $m_{\tilde{\nu}_\tau} \in [1.2, 3]$ TeV but no solution found in this region)
- $|\lambda_{232}| \in [2.5, 3.5]$ (also tried $|\lambda_{232}| \in [1, 2.5]$ but no solution found in this region)
- $m_{\tilde{b}} \in [1.2, 10]$ TeV
- $|\lambda'_{233}| \in [0.01, 3]$
- $|\lambda'_{223}| \in [0.01, 3]$
- $|\lambda'_{232}| \in [0.01, 3]$
- 30 million attempts $\Rightarrow$ 1570 solutions (red+yellow+blue+green points)

Numerical scan

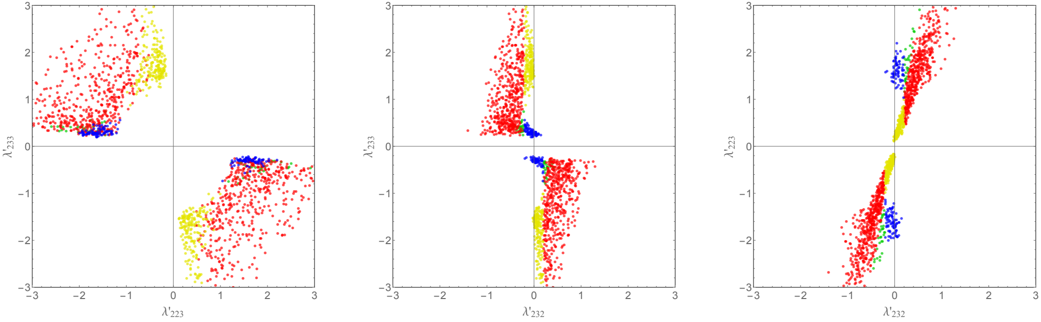

(a) (b) (c)

- Separate to 3 characteristically regions according to Fig(c). Yellow: $|\lambda'_{232}| < 0.2$ and $|\lambda'_{223}| < 1$; Blue: $|\lambda'_{232}| < 0.2$ and $|\lambda'_{223}| > 1$; Red: $|\lambda'_{232}| > 0.2$ and $1.5 < \frac{\lambda'_{223}}{\lambda'_{232}} < 5.5$
- From Fig(c), Red: $\frac{\lambda'_{223}}{\lambda'_{232}} \sim 3 \Leftarrow B_s - \overline{B}_s$ mixing. Green: crossover region from Red to Blue.
- Yellow+Blue: $|\lambda'_{232}|$ small or even zero. Fig(a-c): $|\lambda'_{233}\lambda'_{223}|$ small $\Leftarrow B_s - \overline{B}_s$ mixing.

Numerical scan

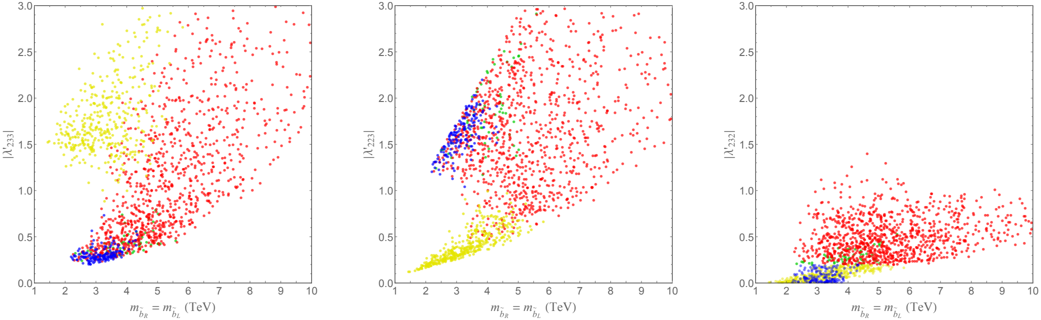

(d) (e) (f)

- Fig(a-c): the absolute sign of λ' not important, only the relative sign matters.
- Fig(e): $\frac{|\lambda'_{223}|}{(m_{\tilde{b}}/1\ \text{TeV})} \lesssim 0.57 \Leftarrow D^0 \to \mu^+\mu^-$; Fig(d): $\frac{|\lambda'_{233}|}{(m_{\tilde{b}}/1\ \text{TeV})} \lesssim 1.0$
- $\Rightarrow$ cannot contribute to $(g-2)_\mu$ much.
- Fig(h): $|\lambda'_{232}| \lesssim 1.5 \Leftarrow$ from Fig(c), $|\lambda'_{232}|$ is either small or $\sim |\lambda'_{223}|/3$

Numerical scan

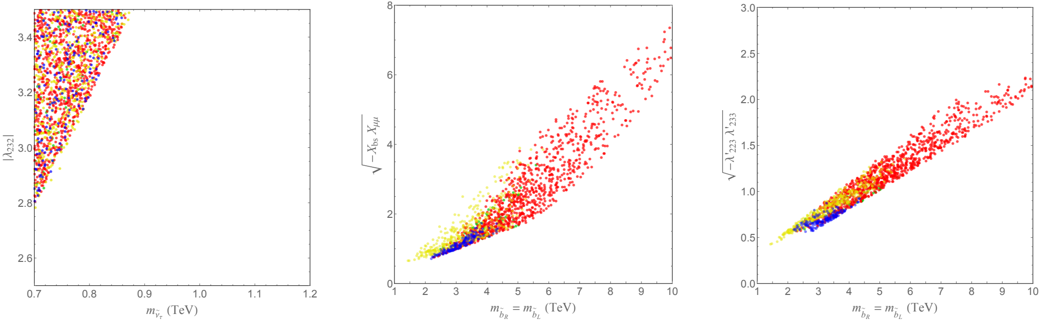

(g) (h) (i)

- Fig(g): Red, Yellow, Blue and Green points are totally mixed $\Leftarrow$ Orthogonality of the two 2-D subspaces: $(\lambda, m_{\tilde{\nu}_\tau})$ and $(\lambda', m_{\tilde{b}})$.
- Fig(h) $\Leftarrow R_{K^{(*)}} \Leftarrow \lambda'_{233}\lambda'_{223} < 0 \Leftarrow$ Fig(a)
- Fig(i): $\dfrac{\sqrt{-\lambda'_{223}\lambda'_{233}}}{(m_{\tilde{b}}/1\ \text{TeV})} \sim (0.2, 0.28) \Leftarrow B \to K\nu\bar{\nu}$

Numerical scan

- Fig(g) $\Rightarrow |\lambda_{232}| \gtrsim 2.78$
- Fig(g) $\Rightarrow 0.70\ \text{TeV} \lesssim m_{\tilde{\nu}_\tau} \lesssim 0.87\ \text{TeV}$
- Fig(d) $\Rightarrow |\lambda'_{233}| \gtrsim 0.20$
- Fig(e) $\Rightarrow |\lambda'_{223}| \gtrsim 0.12$
- Fig(f) $\Rightarrow |\lambda'_{232}|$ could be very small or even zero
- Fig(d-f) $\Rightarrow m_{\tilde{b}} \gtrsim 1.44\ \text{TeV}$
- Fig(g) $\Rightarrow \frac{|\lambda_{232}|}{(m_{\tilde{\nu}_\tau}/1\ \text{TeV})} \gtrsim 4$; Fig(d) $\Rightarrow \frac{|\lambda'_{233}|}{(m_{\tilde{b}_\text{R}}/1\ \text{TeV})} \lesssim 1$; Fig(e) $\Rightarrow \frac{|\lambda'_{223}|}{(m_{\tilde{b}_\text{R}}/1\ \text{TeV})} \lesssim 0.57$. This means that the sneutrino term gives the main contribution of muon (g-2) as one can see from Eq.(3).

Benchmark scenarios

- Density/number of the points in some region $\propto$ the size of the allowed region of the parameter space.
- Three benchmark scenarios:
  - Red scenario (a subset of the Red region in the scatter plot): $\lambda'_{233} = -\lambda'_{223} = -3\lambda'_{232}$, $m_{\tilde{b}_R} = m_{\tilde{b}_L}$, $m_{\tilde{\tau}_L} = 4$ TeV. Fig(c): choose $\lambda'_{223} = -3\lambda'_{232}$ to collect as many red points as possible.
  - Yellow scenario (a subset of the Yellow region in the scatter plot): $\lambda'_{233} = -8\lambda'_{223}$, $\lambda'_{232} = 0$, $m_{\tilde{\tau}_L} = 4$ TeV. Fig(a): $\lambda'_{233} = -8\lambda'_{223}$ to collect as many yellow points as possible.
  - Blue scenario (a subset of the Blue region in the scatter plot): $\lambda'_{223} = -6\lambda'_{233}$, $\lambda'_{232} = 0$, $m_{\tilde{\tau}_L} = 4$ TeV. Fig(a): $\lambda'_{223} = -6\lambda'_{233}$ to collect as many blue points as possible.
  * Red scenario, $\lambda'_{233} = -\lambda'_{223}$ for simplicity.
  * Yellow & Blue scenario, $\lambda'_{232} = 0$ for simplicity $\Rightarrow m_{\tilde{b}_L}, m_{\tilde{t}_L}$ will not appear.

Collider signals

- Signal for $(\lambda', m_{\tilde{b}})$ space: $pp \to \bar{t}\mu^+\mu^-$

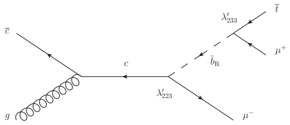

(j)

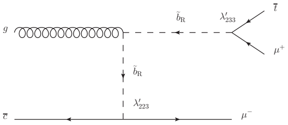

(k)

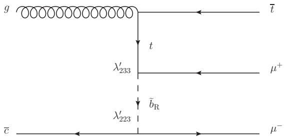

(l)

  - $p_T^{t,\mu} > 20$ GeV, $|\eta^{t,\mu}| < 2.5$, $\Delta R^{\mu\mu} > 0.4$ and $\Delta R^{t\mu} > 0.4$, $M_{\mu^+\mu^-} > 0.4$ TeV. Assume $\mathscr{L} = 3000\ \mathrm{fb}^{-1}$. $\sqrt{s} = 14\ \mathrm{TeV}, 27\ \mathrm{TeV}, 100\ \mathrm{TeV}$.
  - Background small. $pp \to \bar{t}\mu^+\mu^- X$ (with $X = j, b, W^+ \to jj, W^+ \to \ell^+\nu_\ell$ not detected: $p_T^{j,b,l} < 20$ GeV, $E_T^{\mathrm{miss}} < 20$ GeV)
  - $pp \to t\mu^+\mu^-$ is similar but with a larger background.
  - Only λ'_{233}, λ'_{223} and $m_{\tilde{b}_R}$ contribute to the signal. What can be probed are actually these parameters, a projection of the scenario.

Collider signals

- Signal for $(\lambda, m_{\widetilde{\nu}_\tau})$ space: $pp \to \mu^+\mu^-\mu^+\mu^-$

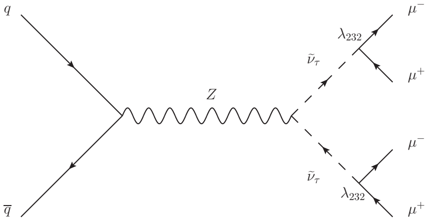

(m)

- $p_{\mathrm{T}}^{\mu} > 25$ GeV, $|\eta^\mu| < 2.47$, $\Delta R^{\mu\mu} > 0.2$, $M_{\mu^+\mu^-} > 0.4$ TeV.
- Assume the mass of the lightest neutralino is 100 GeV for the calculation of the branching ratio of $\widetilde{\nu}_\tau$. $\mathrm{BR}(\widetilde{\nu}_\tau \to \mu^+\mu^-)$ is larger than 95% when $|\lambda_{232}| > 1.2$

Anomalies and constraints (Red scenario)

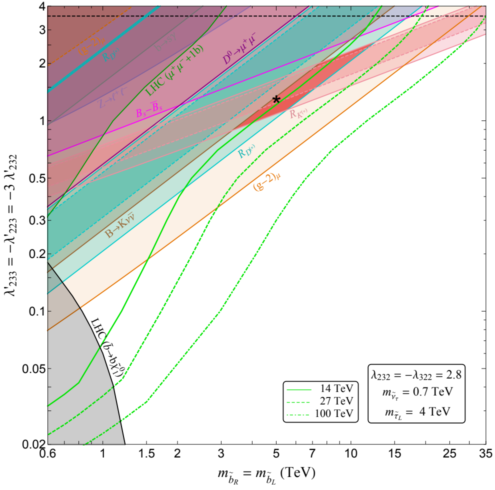

(n)

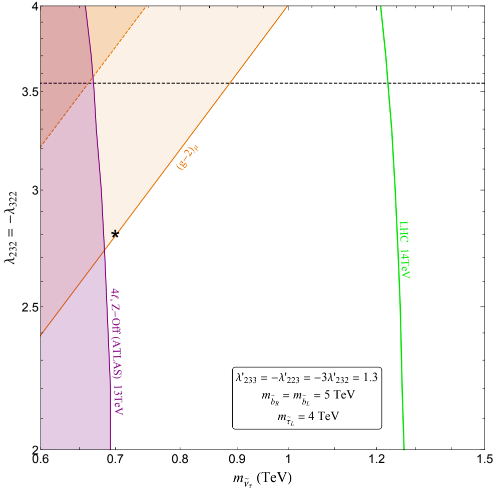

(o)

Anomalies and constraints (Yellow scenario)

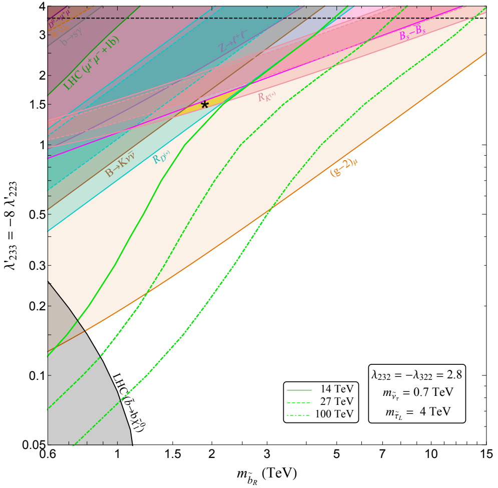

(p)

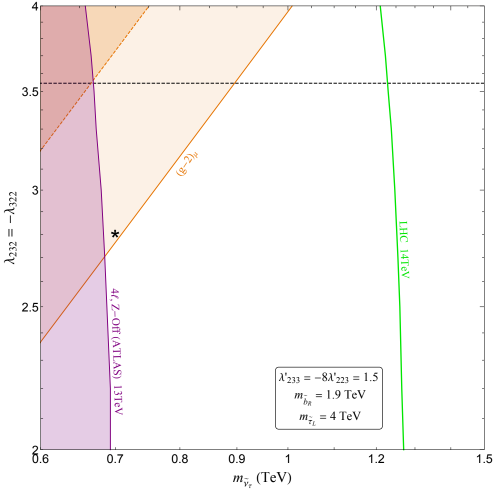

(q)

Anomalies and constraints (Blue scenario)

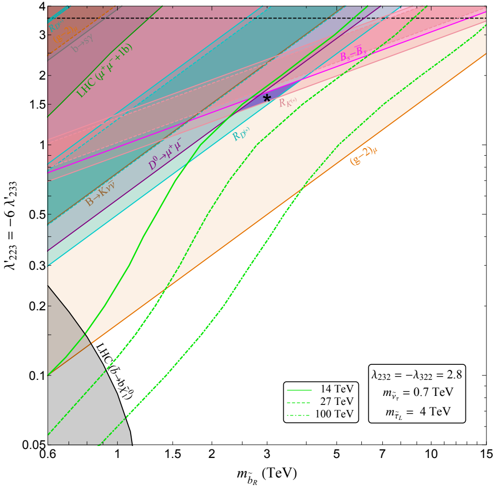

(r)

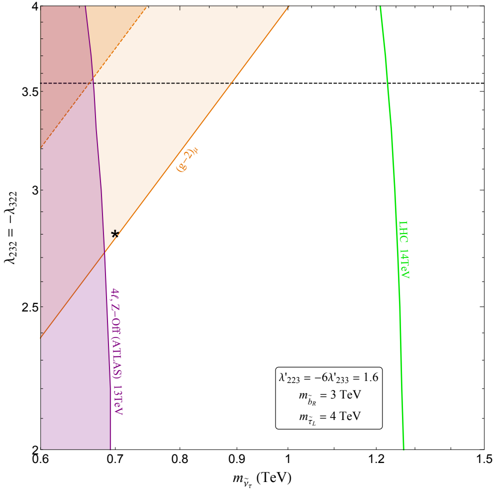

(s)

Discussions

- The figure on the left uses the value of the black star in the figure on the right and vice versa.
- The cyan, pink and orange shaded regions with solid (dashed) boundaries explain the $R_{D^{(*)}}$, $R_{K^{(*)}}$ and $(g-2)_\mu$ anomalies at 3σ (2σ) CL respectively.
- The red, yellow and blue shaded regions are the overlap regions that simultaneously explain all the three anomalies correspond to the red, yellow and blue scenarios.
- The green solid, dashed and dot-dashed lines in Fig(n)(p)(r) are the 2σ sensitivities of the $\sqrt{s}=$ 14 TeV, 27 TeV and 100 TeV pp colliders in the $\bar{t}\mu^+\mu^-$ channel.
- These green curves bend downward at large λ' region because of the off-shell contribution of $pp \to \bar{t}\mu^+\mu^-$ Fig(l).
- The green solid line in Fig(o)(q)(s) are the 2σ sensitivities of the LHC 14 TeV in the 4-muon channel.
- Fig(o)(q)(s) are quite similar. Consistent with Fig(g). Consequence of the orthogonality of the two subspaces $(\lambda, m_{\tilde{\nu}_\tau})$ and $(\lambda', m_{\tilde{b}})$

Discussions

- In the yellow and blue scenarios, we can allow a non-zero λ'_{232} (correspond to the yellow and blue points out of the vertical axis in Fig(b,c)). And this will make the $B_s - \overline{B}_s$ mixing constraint weaker and enlarge the allowed parameter space for $R_{K^{(*)}}$.
- We choose the black stars that are very close to the 3σ lower bound of $(g-2)_\mu$ in Fig(o)(q)(s) to show the dependence of $(g-2)_\mu$ from $(\lambda', m_{\widetilde{b}})$ in Fig(n)(p)(r). Otherwise, the 3σ lower bound of $(g-2)_\mu$ will disappear in Fig(n)(p)(r) because the contribution from $\widetilde{b}$ is much smaller compared with $\widetilde{\nu}_\tau$.
- $B_s \to \mu^+\mu^-$ is always satisfied once $R_{K^{(*)}}$ is explained. Even if we take the extreme 3σ value, $|(C_{10})^\mu - (C'_{10})^\mu| = 0.89$ (Altmannshofer, Stangl (arXiv:2103.13370)). This implies the RPV contribution $< 1.4 \times 10^{-10}$ (Becirevic, Fajfer, Kosnik (PRD 2015)) while the current experimental value is BR$(B_s \to \mu^+\mu^-) = (3.0 \pm 0.4) \times 10^{-9}$
- The lower bound of $m_{\widetilde{\nu}_\tau}$ comes from the recast of the 4-lepton search of ATLAS (ATLAS-CONF-2021-011). The 4-lepton signal in our scenario comes from the pair production of $\widetilde{\nu}_\tau$ with $\widetilde{\nu}_\tau \to \mu^+\mu^-$.

Summary

- We suggest that in RPV3 SUSY:
  - A $\widetilde{b}$ with mass $\sim 2 - 12$ TeV and non-zero couplings λ'_{233}, λ'_{223} and λ'_{232} could explain $R_{D^{(*)}}$ and $R_{K^{(*)}}$ anomalies at 3σ CL (especially even 1σ for $R_{K^{(*)}}$) while having a little bit contribution on $(g-2)_\mu$ anomaly due to the constraints of $B \to K^{(*)}\nu\overline{\nu}$, $B_s - \overline{B}_s$ mixing etc.;
  - A $\widetilde{\nu}_\tau$ with mass $\sim 0.7 - 1$ TeV and non-zero coupling $|\lambda_{232}| \gtrsim 2.7$ could explain $(g-2)_\mu$ anomaly at 3σ CL.
  - Both $(m_{\widetilde{b}}, \lambda')$ and $(m_{\widetilde{\nu}_\tau}, \lambda)$ parameter spaces are (partly) testable at HL-LHC through $\bar{t}\mu^+\mu^-$ or four muon signals.
  - Due to the orthogonality between $(m_{\widetilde{b}}, \lambda')$ and $(m_{\widetilde{\nu}_\tau}, \lambda)$ in the sense of the solutions of anomalies, even if the $(m_{\widetilde{b}}, \lambda')$ solution is ruled out by the signal we proposed or future low energy constraints, the $(m_{\widetilde{\nu}_\tau}, \lambda)$ solution is still valid and vice versa.

Supplementary material

Backup

Choice of the couplings

- $(g-2)_\mu \Rightarrow$ candidates from Eq.(3): $\lambda_{312}, \lambda_{321}, \lambda_{322}, \lambda_{323}$ (λ'_{2k3} terms cannot contribute much). To get enough contribution, we have to let at least two λ couplings to be non-zero otherwise the magnitude of the λ need to be larger than $\sqrt{4\pi}$.
- $\checkmark$ $\lambda_{322} \neq 0$, contributes two times for $k=2$ in Eq.(3)
- $\times$ $\lambda_{323} \neq 0$, need to add another coupling to get enough contribution. But $\tau \to \overline{e}\mu\mu \Rightarrow \lambda_{323}\lambda_{312}$ small (propagator $\widetilde{\nu}_\tau$); $\tau \to e\mu\overline{\mu} \Rightarrow \lambda_{323}\lambda_{321}$ small (propagator $\widetilde{\nu}_\tau$); $\tau \to \mu\mu\overline{\mu} \Rightarrow \lambda_{323}\lambda_{322}$ small (propagator $\widetilde{\nu}_\tau$).
- ? $\lambda_{312} \neq 0$ and $\lambda_{321} \neq 0$, cannot let $\lambda_{322} \neq 0$ at the same time due to the constraint of $\mu \to e\gamma$
- $\times$ $\lambda'_{3ij} \neq 0$ moreover, because $(\overline{d}_i d_j) \to \mu\overline{\mu} \Rightarrow \lambda_{322}\lambda'_{3ij}$ small (propagator $\widetilde{\nu}_\tau$).

Choice of couplings

- $R_{K^{(*)}} \Rightarrow \lambda'_{233}\lambda'_{223} \neq 0$ since $\lambda'_{3ij} \approx 0$ and $\lambda_{323} \approx 0$
- ✓ $\lambda'_{233} \neq 0$ and $\lambda'_{223} \neq 0$. Only choice of $R_{K^{(*)}}$, also contribute to $R_{D^{(*)}}$
- $\lambda'_{ij3} \neq 0$ and $\lambda'_{i3j} \neq 0$ may cause some troubles because
  $(\overline{u}_j c) \to \overline{e}_i \mu \Rightarrow \lambda'_{223}\lambda'_{ij3}$ (propagator $\widetilde{b}_{\mathrm{R}}$) e.g. $D^0 \to \mu^+\mu^- \Rightarrow \frac{\lambda'_{213}}{m^2_{\widetilde{b}_{\mathrm{R}}}}$ small;
  $(\overline{d}_j b) \to \overline{e}_i \mu \Rightarrow \lambda'_{233}\lambda'_{i3j}$ (propagator $\widetilde{t}_{\mathrm{L}}$) e.g. $B_s \to \mu^+\mu^- \Rightarrow \frac{\lambda'_{232}}{m^2_{\widetilde{t}_{\mathrm{L}}}}$ small.
- In our case $\lambda'_{232} \neq 0$. But a small λ'_{232} may also be possible (but the cancellation term in $B_s - \overline{B}_s$ mixing is zero) and λ'_{232} will contribute to $B_s \to \mu^+\mu^-$, $(C'_9)^\mu$ and $(C'_{10})^\mu$. But λ'_{232} do not have to be small and prefer the relation $\lambda'_{223} \approx 3\lambda'_{232}$.
- Now, non-zero couplings are chosen to be λ_{232}, λ'_{233}, λ'_{223} and λ'_{232}.

Background cross-section

- $pp \to t\mu^+\mu^-$ has a larger background cross-section because the u content in proton is much larger than the $\overline{u}$ content.
- We can look for $t\mu^+\mu^-$ or even combine both, but the result should be similar because the signal of $t\mu^+\mu^-$ is nearly the same as $\bar{t}\mu^+\mu^-$.

Table 1: $pp \to \bar{t}\mu^+\mu^- X$ cross sections (fb)

X	14 TeV	$M_{\mu^+\mu^-} > 0.15$ TeV	27 TeV	$M_{\mu^+\mu^-} > 0.15$ TeV	100 TeV	$M_{\mu^+\mu^-} > 0.15$ TeV
j	0.381	3.35×10^{-3}	1.06	1.05×10^{-2}	5.83	7.11×10^{-2}
b	4.23×10^{-3}	3.64×10^{-5}	9.47×10^{-3}	9.85×10^{-5}	3.84×10^{-2}	3.92×10^{-4}
$W^+ \to jj$	3.76×10^{-3}	2.75×10^{-5}	1.49×10^{-2}	1.33×10^{-4}	0.133	1.58×10^{-3}
$W^+ \to e^+\nu_e$	6.38×10^{-4}	5.68×10^{-6}	2.53×10^{-3}	2.68×10^{-5}	2.24×10^{-2}	2.28×10^{-4}
$W^+ \to \mu^+\nu_\mu$	6.15×10^{-3}	2.67×10^{-3}	2.64×10^{-2}	1.12×10^{-2}	0.242	0.120
$W^+ \to \tau^+\nu_\tau$	6.34×10^{-4}	6.09×10^{-6}	2.52×10^{-3}	3.08×10^{-5}	2.25×10^{-2}	2.81×10^{-4}
Total	0.396	6.10×10^{-3}	1.12	2.20×10^{-2}	6.29	0.194

[a] $p_T^{j,b,l} < 20$ GeV, $E_T^{\text{miss}} < 20$ GeV
[b] $p_T^{t,\mu} > 20$ GeV, $| \eta^{t,\mu} | < 2.5$

Invariant mass distribution (Red scenario)

- For the process $pp \to \bar{t}\mu^+\mu^-$
- Invariant mass $M_{\mu^+\mu^-}$ distributions at $\sqrt{s} = 14\ \mathrm{TeV}, 27\ \mathrm{TeV}, 100\ \mathrm{TeV}$

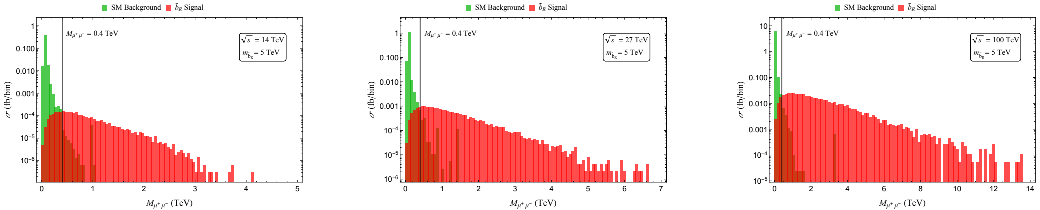

- We have used $\lambda'_{233} = -\lambda'_{223} = 1.3$, $m_{\tilde{b}_R} = 5\ \mathrm{TeV}$ for the signal process (the black star in Fig(n)).

Invariant mass distribution (Yellow scenario)

- For the process $pp \to \bar{t}\mu^+\mu^-$
- Invariant mass $M_{\mu^+\mu^-}$ distributions at $\sqrt{s} = 14\ \text{TeV}, 27\ \text{TeV}, 100\ \text{TeV}$

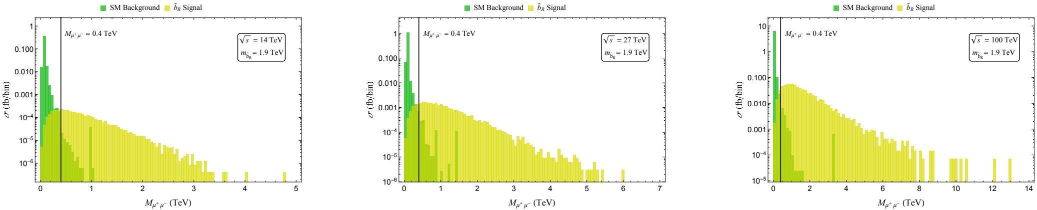

- We have used $\lambda'_{233} = -8\lambda'_{223} = 1.5$, $m_{\tilde{b}_R} = 1.9\ \text{TeV}$ for the signal process (the black star in Fig(p)).

Invariant mass distribution (Blue scenario)

- For the process $pp \to \bar{t}\mu^+\mu^-$
- Invariant mass $M_{\mu^+\mu^-}$ distributions at $\sqrt{s} = 14\ \mathrm{TeV}, 27\ \mathrm{TeV}, 100\ \mathrm{TeV}$

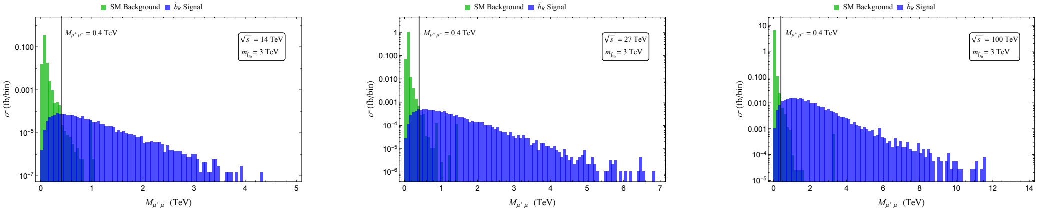

- We have used $\lambda'_{223} = -6\lambda'_{233} = 1.6$, $m_{\tilde{b}_{\mathrm{R}}} = 3\ \mathrm{TeV}$ for the signal process (the black star in Fig(r)).

Anomalies and constraints (Red scenario)

- Since many anomalies and constraints are independent of $(\lambda_{232}, m_{\tilde{\nu}_\tau})$, they become just numbers instead of curves in Fig(o).

Anomaly/Constraint	Quantities in Figure(m)	Experimental value/limit
$R_{D^{(*)}}$	$\frac{R_{D^{(*)}}}{R^{\rm SM}_{D^{(*)}}} = 1.05$	1.15 ± 0.04
$R_{K^{(*)}}$	$(C_9)^\mu = -(C_{10})^\mu = -0.23$	-0.35 ± 0.08
$D^0 \to \mu^+\mu^-$	$\text{BR}(D^0 \to \mu^+\mu^-) = 2.8 \times 10^{-10}$	$< 7.6 \times 10^{-9}$ (95% CL)
$B \to K^{(*)}\nu\overline{\nu}$	$R_{B\to K^{(*)}\nu\overline{\nu}} = \frac{\text{BR}(B\to K^{(*)}\nu\overline{\nu})}{\text{BR}_{\rm SM}(B\to K^{(*)}\nu\overline{\nu})} = 4.6$	< 5.2 (95% CL)
$B_s - \overline{B}_s$ mixing	$\Delta M_{B_s} = (20.1 \pm 1.7)\ \text{ps}^{-1}$	$(17.757 \pm 0.021)\ \text{ps}^{-1}$
$B_s \to \mu^+\mu^-$	$< 9.1 \times 10^{-12}$	$(3.0 \pm 0.4) \times 10^{-9}$

Anomalies and constraints (Yellow scenario)

- Since many anomalies and constraints are independent of $(\lambda_{232}, m_{\tilde{\nu}_\tau})$, they become just numbers instead of curves in Fig(q).

Anomaly/Constraint	Quantities in Figure(o)	Experimental value/limit
$R_{D^{(*)}}$	$\frac{R_{D^{(*)}}}{R_{D^{(*)}}^{\rm SM}} = 1.04$	1.15 ± 0.04
$R_{K^{(*)}}$	$(C_9)^\mu = -(C_{10})^\mu = -0.13$	-0.35 ± 0.08
$D^0 \to \mu^+\mu^-$	$\mathrm{BR}(D^0 \to \mu^+\mu^-) = 2.6 \times 10^{-12}$	$< 7.6 \times 10^{-9}$ (95% CL)
$B \to K^{(*)}\nu\overline{\nu}$	$R_{B\to K^{(*)}\nu\overline{\nu}} = \frac{\mathrm{BR}(B\to K^{(*)}\nu\overline{\nu})}{\mathrm{BR_{SM}}(B\to K^{(*)}\nu\overline{\nu})} = 3.3$	< 5.2 (95% CL)
$B_s - \overline{B}_s$ mixing	$\Delta M_{B_s} = (22.4 \pm 1.7)\ \mathrm{ps}^{-1}$	$(17.757 \pm 0.021)\ \mathrm{ps}^{-1}$
$B_s \to \mu^+\mu^-$	3.0×10^{-12}	$(3.0 \pm 0.4) \times 10^{-9}$

Anomalies and constraints (Blue scenario)

- Since many anomalies and constraints are independent of $(\lambda_{232}, m_{\tilde{\nu}_\tau})$, they become just numbers instead of curves in Fig(s).

Anomaly/Constraint	Quantities in Figure(q)	Experimental value/limit
$R_{D^{(*)}}$	$\frac{R_{D^{(*)}}}{R^{\rm SM}_{D^{(*)}}} = 1.03$	1.15 ± 0.04
$R_{K^{(*)}}$	$(C_9)^\mu = -(C_{10})^\mu = -0.13$	-0.35 ± 0.08
$D^0 \to \mu^+\mu^-$	$\mathrm{BR}(D^0 \to \mu^+\mu^-) = 5.4 \times 10^{-9}$	$< 7.6 \times 10^{-9}$ (95% CL)
$B \to K^{(*)}\nu\overline{\nu}$	$R_{B\to K^{(*)}\nu\overline{\nu}} = \frac{\mathrm{BR}(B\to K^{(*)}\nu\overline{\nu})}{\mathrm{BR}_{\rm SM}(B\to K^{(*)}\nu\overline{\nu})} = 1.3$	< 5.2 (95% CL)
$B_s - \overline{B}_s$ mixing	$\Delta M_{B_s} = (22.2 \pm 1.7)\ \mathrm{ps}^{-1}$	$(17.757 \pm 0.021)\ \mathrm{ps}^{-1}$
$B_s \to \mu^+\mu^-$	2.8×10^{-12}	$(3.0 \pm 0.4) \times 10^{-9}$